PNAS RESEARCH ARTICLE | IMMUNOLOGY AND INFLAMMATION OPEN ACCESS

IL-6/gp130 signaling in CD4$^+$ T cells drives the pathogenesis of pulmonary hypertension

Tomohiko Ishibashi[a,1], Tadakatsu Inagaki[a,1], Makoto Okazawa[a], Akiko Yamagishi[a], Keiko Ohta-Ogo[b], Ryotaro Asano[a,c], Takeshi Masaki[a], Yui Kotani[a], Xin Ding[a], Tomomi Chikaishi-Kirino[a], Noriko Maedera[a], Manabu Shirai[d], Kinta Hatakeyama[b], Yoshiaki Kubota[e], Tadamitsu Kishimoto[f,2], and Yoshikazu Nakaoka[a,c,g,h,2]

Contributed by Tadamitsu Kishimoto; received September 19, 2023; accepted March 7, 2024; reviewed by Tak W. Mak and Ruslan Medzhitov

Pulmonary arterial hypertension (PAH) is characterized by stenosis and occlusions of small pulmonary arteries, leading to elevated pulmonary arterial pressure and right heart failure. Although accumulating evidence shows the importance of interleukin (IL)-6 in the pathogenesis of PAH, the target cells of IL-6 are poorly understood. Using mice harboring the *floxed* allele of *gp130*, a subunit of the IL-6 receptor, we found substantial Cre recombination in all hematopoietic cell lineages from the primitive hematopoietic stem cell level in *SM22α-Cre* mice. We also revealed that a CD4$^+$ cell-specific gp130 deletion ameliorated the phenotype of hypoxia-induced pulmonary hypertension in mice. Disruption of IL-6 signaling via deletion of *gp130* in CD4$^+$ T cells inhibited phosphorylation of signal transducer and activator of transcription 3 (STAT3) and suppressed the hypoxia-induced increase in T helper 17 cells. To further examine the role of IL-6/gp130 signaling in more severe PH models, we developed *Il6* knockout (KO) rats using the CRISPR/Cas9 system and showed that IL-6 deficiency could improve the pathophysiology in hypoxia-, monocrotaline-, and Sugen5416/hypoxia (SuHx)-induced rat PH models. Phosphorylation of STAT3 in CD4$^+$ cells was also observed around the vascular lesions in the lungs of the SuHx rat model, but not in *Il6* KO rats. Blockade of IL-6 signaling had an additive effect on conventional PAH therapeutics, such as endothelin receptor antagonist (macitentan) and soluble guanylyl cyclase stimulator (BAY41-2272). These findings suggest that IL-6/gp130 signaling in CD4$^+$ cells plays a critical role in the pathogenesis of PAH.

pulmonary arterial hypertension | interleukin-6 | CD4$^+$ T cell | inflammation | *SM22α-Cre*

Significance

IL-6 signaling has a pivotal role in the pathogenesis of pulmonary arterial hypertension (PAH). However, the target cells of IL-6 signaling in PAH have been elusive. Here, we revealed that *SM22α-Cre* mice show unexpected recombination in almost all hematopoietic cell lineages. Based on these findings, we demonstrated that IL-6/gp130 signaling in CD4$^+$ T cells has a critical role in the pathogenesis of PAH. We next examined the effects of *Il6* deletion on severe PAH models in rats and showed that IL-6 deficiency improves the pathophysiology in several rat PAH models. Furthermore, the additive effect of IL-6 deficiency with existing PAH therapies was also revealed. Taken together, IL-6/gp130 signaling in CD4$^+$ cells is important in the pathogenesis of PAH.

Pulmonary arterial hypertension (PAH) is characterized by stenosis and occlusions of small pulmonary arteries, leading to elevated pulmonary arterial pressure and right heart failure. The importance of inflammation in the pathogenesis of PAH has been reported (1, 2). Interleukin (IL)-6 is a multifunctional proinflammatory cytokine linked to numerous autoimmune diseases (3, 4). The serum level of IL-6 increased in patients with idiopathic PAH, and the IL-6 level correlated with prognosis (5). In animal studies, it has been reported that transgenic mice overexpressing IL-6 exhibit manifestations of pulmonary hypertension (PH) pathology even under conditions of normoxia and that these manifestations are exacerbated by chronic hypoxia (6). Furthermore, it has been reported that the manifestations of hypoxia-induced pulmonary hypertension (HPH) were improved in IL-6-deficient mice (7).

We reported that inhibiting the IL-6 signal by MR16-1, an anti-mouse IL-6 receptor antibody, resulted in a significant improvement in the HPH phenotype (8). We also reported that the Pristane/Hypoxia model, a mouse PAH model that reflects the pathological features of connected tissue disease-associated PAH, is IL-6 dependent and that the phenotype of this model was ameliorated by MR16-1 (9). In addition, we found an association between the upstream molecules that regulate IL-6 expression and the pathogenesis of PAH. Regnase-1, encoded by the *ZC3H12A* gene, regulates the expression levels of various inflammatory cytokines, including IL-6, by degrading their mRNAs (10). We have recently reported that *ZC3H12A* expression in peripheral blood mononuclear cells was decreased in patients with PAH, and its expression is inversely correlated with disease severity (11). Furthermore, mice lacking Regnase-1 in alveolar macrophages spontaneously developed severe PAH without hypoxic exposure (11). These findings strongly indicate the significant role of Regnase-1 in the pathophysiology of PAH. However, the target cells of IL-6 are largely unknown. Two studies have analyzed the significance of IL-6 signaling in smooth muscle cells (SMCs) in the pathogenesis of PAH by deleting the IL-6-specific receptor alpha subunit (IL-6Rα), which triggers the IL-6 signaling in association with the IL-6 signal transduction (IL6ST, also called gp130), specifically in the smooth muscle

Author contributions: T. Ishibashi, T. Inagaki, T.K., and Y.N. designed research; T. Ishibashi, T. Inagaki, A.Y., K.O.-O., R.A., T.M., Y. Kotani, X.D., T.C.-K., N.M., and M.S. performed research; T. Ishibashi, T. Inagaki, M.O., A.Y., K.O.-O., T.C.-K., N.M., K.H., Y. Kubota, T.K., and Y.N. analyzed data; and T. Ishibashi, T. Inagaki, and Y.N. wrote the paper.

Reviewers: T.W.M., University of Toronto; and R.M., Yale University.

Competing interest statement: Y.N. reports consulting fees from Chugai Pharmaceutical Co., Ltd. outside the submitted work; consulting fees from Janssen Pharmaceutical K.K. outside the submitted work.

[1]T. Ishibashi and T. Inagaki contributed equally to this work.

[2]To whom correspondence may be addressed. Email: kishimoto@ifrec.osaka-u.ac.jp or ynakaoka@ncvc.go.jp.

This article contains supporting information online at https://www.pnas.org/lookup/suppl/doi:10.1073/pnas.2315123121/-/DCSupplemental.

Published April 11, 2024.

lineage (12, 13). One study used *SM22α-Cre*, an SMC-specific *Cre* mouse model, and reported that IL-6 signaling in SMCs acts as an aggravating factor to promote vascular remodeling in PAH (13). The second study used *SMMHC-CreERT2*, another SMC-specific Cre mouse model, and concluded that IL-6 signaling in SMCs is protective against Schistosoma- and hypoxia-induced PH (12). This difference may be due to several factors: *SM22α-Cre* causes a defect in IL-6 signaling via IL-6Ra in SMCs from birth, whereas *SMMHC-CreERT2* causes a defect in the IL-6Ra only after tamoxifen administration. The authors also discuss the possibility that the altitude of the experimental facility may have affected the results (12). However, differences in tissue specificity of *Cre* mice and Cre recombination in nonspecific organs also need to be noted. The *SM22α-Cre* (14) mouse is one of the SMC-specific Cre transgenic mice that is widely used in the field of vascular biology for vascular SMC-specific gene knockout and reporter purposes. However, a previous report has shown that unintentional Cre recombination also occurs in some myeloid lineage cells in *SM22α-Cre* mice (15). The mice have been used to study the pathogenesis of various diseases, including atherosclerosis (14), hypertension (16), aneurysms (17), and PH (13, 18).

Here, we investigated the tissue specificity of *SM22α-Cre* mice and found substantial Cre recombination in all hematopoietic cell lineages from the primitive hematopoietic stem cell level. Based on these results and the expression pattern of gp130, we proposed that IL-6/gp130 signaling in $CD4^+$ T cells was important in the pathogenesis of PAH. To further examine the role of IL-6/gp130 signaling in more severe PH models, we developed *Il6* knockout (KO) rats using the CRISPR/Cas9 system and showed that IL-6 deficiency could improve the pathophysiology in several rat PAH models including the Sugen5416/hypoxia model.

Results

Disruption of IL-6 Signaling via gp130 Deletion Using *SM22α-Cre* Resulted in an Improvement in the Pulmonary Hypertension (PH) Phenotype of an HPH Mouse Model. To clarify the effect of tissue-specific gp130 deficiency on the phenotypes of HPH, we crossed *gp130flox* (19) mice with three tissue-specific *Cre* mice, *VE-Cad-CreERT2* (20) (for endothelial cells), *SMMHC-CreERT2* (12, 21), and *SM22α-Cre* mice (13, 16) (for SMCs), and subjected these mice to 4 wk of hypoxia (Fig. 1*A*). Tamoxifen was administered intraperitoneally to induce Cre recombination in *CreERT2* mice. In wild-type (WT) mice, 4 wk of hypoxia resulted in elevated right ventricular systolic pressure (RVSP) and an increase in Fulton's index (Fig. 1 *B* and *C*). These elevations were also observed in mice with only the *floxed gp130* allele and not *Cre*. Endothelial cell-specific gp130 deficiency induced by *VE-Cad-CreERT2* mice did not improve the RVSP or Fulton's index (Fig. 1 *B* and *C*). Two types of SMC-targeted Cre mice showed conflicting results. While deletion of gp130 using *SMMHC-CreERT2* mice did not ameliorate the phenotype of HPH, deletion of gp130 using *SM22α-Cre* mice improved the RVSP (Fig. 1 *B* and *C*).

***SM22α-Cre* Mice Produced an Unexpected Cre Recombination in Hematopoietic Cells.** The discrepancy between the results obtained in the two SMC-targeted Cre mice was similar to that in previous reports (12, 13). One previous report showed that unintentional Cre recombination also occurs in some myeloid lineage cells in *SM22α-Cre* mice (15). We hypothesized that the discrepancy in the results of the two SMC-targeted Cre mice may be due to nonspecific Cre recombination in *SM22α-Cre* mice. To analyze Cre recombination in the hematopoietic lineage cells of *SMMHC-CreERT2* and *SM22α-Cre* mice in detail, we generated

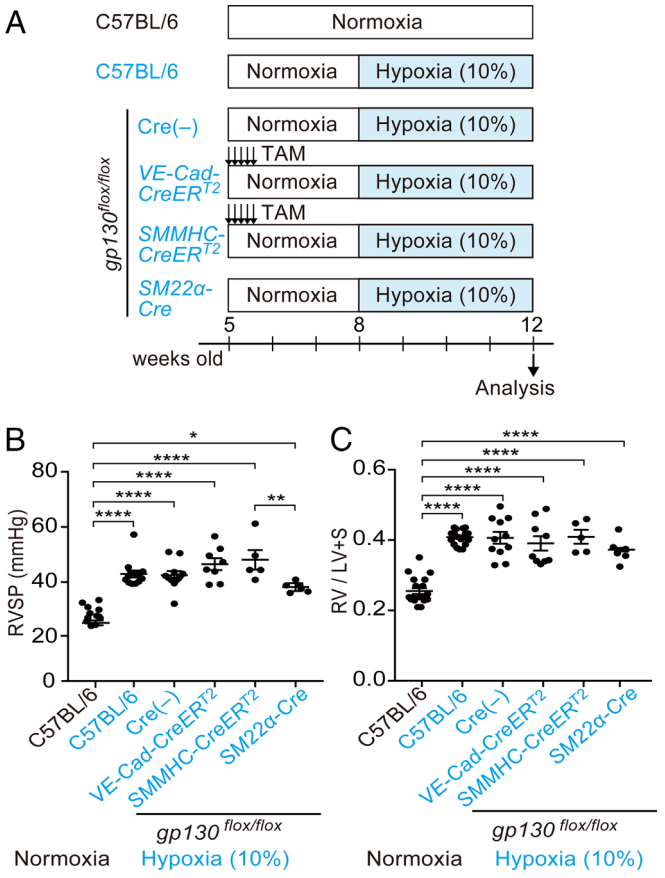

Fig. 1. Gp130 deletion using *SM22α-Cre* showed a tendency to improve pulmonary hypertension in the HPH mouse model. (*A*) Experimental protocols and the groups are shown. Male 8-wk-old mice were exposed to a 10% hypoxic chamber for 4 wk. To induce *CreERT2*-mediated Cre recombination, 1 mg of tamoxifen was injected intraperitoneally on 5 consecutive days. (*B*) Right ventricular systolic pressure (RVSP) of each group is shown. (*C*) Right ventricle/left ventricle + septum (RV/LV+S) weight ratio (Fulton's index) of each group is shown.

reporter mice by crossing *Rosa26-loxP-stop-loxP-tdTomato* mice (22), which express tdTomato fluorescence by Cre recombination, with *SMMHC-CreERT2* or *SM22α-Cre* mice (*SI Appendix*, Fig. S1 *A* and *B*). Using these reporter mice, we were able to visualize the Cre recombinant cells with tdTomato fluorescence.

In the bone marrow of *SMMHC-CreERT2* reporter mice, Cre recombination (tdTomato-positive cells) was observed in the vascular SMCs surrounding the arteries in the bone marrow (Fig. 2*A*). Flow cytometry analysis of hematopoietic cells from the bone marrow and spleen of *SMMHC-CreERT2* mice showed that Cre recombination did not occur in the hematopoietic cell lineage (Fig. 2*B*).

By contrast, *SM22α-Cre* reporter mice showed different results. As expected, Cre recombination occurred in the SMCs of the gastrointestinal tract and in the vascular SMCs of the aorta (*SI Appendix*, Fig. S1 *C–E*). Regarding the bone marrow, Cre recombination did occur in the SMCs surrounding the arteries in the bone marrow. However, tdTomato-positive cells, which experienced Cre recombination, were also widely found in hematopoietic cells around the bone marrow (Fig. 2*C*). Flow cytometric analysis also confirmed Cre recombination in CD45-positive hematopoietic cells of the bone marrow and spleen (Fig. 2*D*).

To examine the difference in Cre recombination depending on the hematopoietic cell lineage, the tdTomato positive rates of myeloid cells, T cells, and B cells in peripheral blood from *SM22α-Cre* reporter mice were analyzed by flow cytometry (*SI Appendix*, Fig. S2 *A* and *B*).

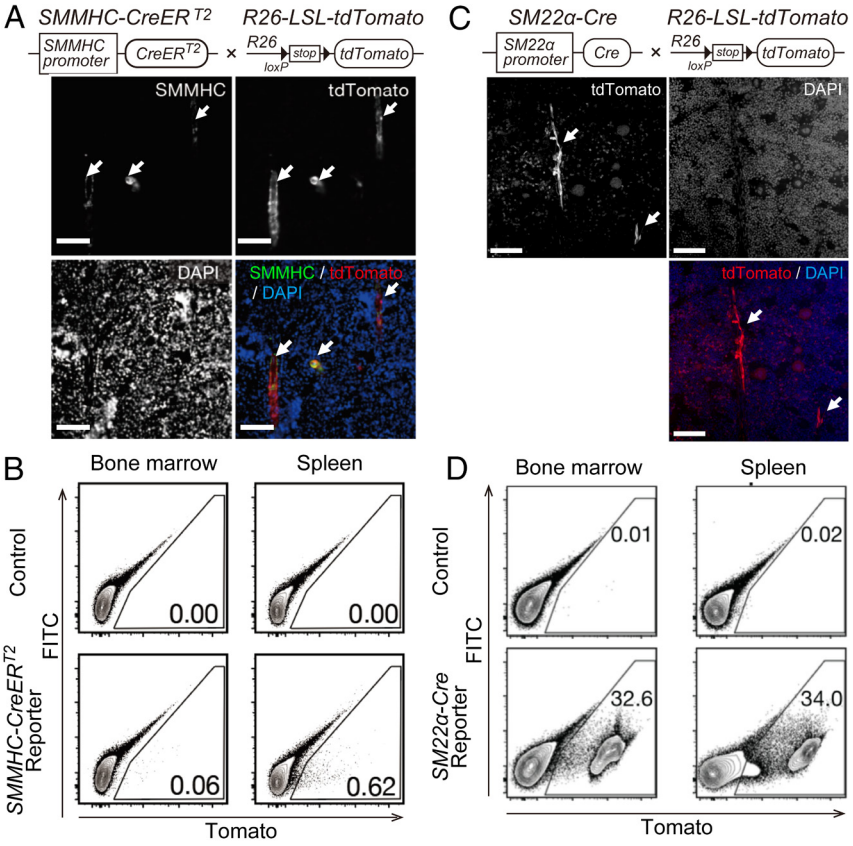

Fig. 2. Unintended Cre recombination in all hematopoietic lineage cells in *SM22α-Cre* mice. (*A*) Representative image of immunofluorescence staining of the bone marrow from *SMMHC-CreERT2* reporter mice. The arrows indicate smooth muscle cells around arteries in the bone marrow. *SMMHC-CreERT2* mice were crossed with *Rosa26-loxP-stop-loxP-tdTomato* mice. (*B*) Flow cytometry analysis of hematopoietic tissues from *SMMHC-CreERT2* reporter mice. FITC channels were used to remove cells that emit nonspecific autofluorescence. Gates indicate tdTomato-positive cells, and the percentages of cells in each gate are shown in each panel. (*C*) Representative image of immunofluorescence staining of the bone marrow from *SM22α-Cre* reporter mice. The arrows indicate smooth muscle cells around arteries in the bone marrow. *SM22α-Cre* mice were crossed with *Rosa26-loxP-stop-loxP-tdTomato* mice. (*D*) Flow cytometry analysis of hematopoietic tissues from *SM22α-Cre* reporter mice. FITC channels were used to remove cells that emit nonspecific autofluorescence. Gates indicate tdTomato-positive cells, and the percentages of cells in each gate are shown in each panel.

Cre recombination was observed in all three lineages, but the ratio of Cre recombination was significantly higher in myeloid cells compared with lymphoid cells (*SI Appendix*, Fig. S2*C*). Regarding stem/progenitor cells, Cre recombination was observed at a low rate at the hematopoietic stem cell level, the most undifferentiated hematopoietic cell lineage (*SI Appendix*, Fig. S2 *D* and *E*). As the differentiation of blood cells progressed, an increase in the Cre recombination ratio was observed (*SI Appendix*, Fig. S2*F*). Cre recombination was also observed in the myeloid and lymphoid progenitor cells in the bone marrow (*SI Appendix*, Fig. S2 *G–I*). These results indicated that *SM22α-Cre* mice showed nonspecific Cre recombination in blood cells, suggesting that the improvement in HPH phenotype in *gp130flox/flox; SM22α-Cre* mice might be due to nonspecific gp130 deletion in blood cells.

***SM22α-Cre* Mice Had Partially Deleted gp130 in CD4$^+$ Cells after Crossing with *gp130 flox* Mice.** Using publicly available data to examine the expression of gp130 in differentiation stages of blood cells (23), we found that in mature blood cells, gp130 expression is particularly high in T cells (Fig. 3*A*). Indeed, gp130 was highly expressed on CD3ε$^+$ CD4$^+$ T cells in the spleen of control *gp130flox/flox* mice (Fig. 3*B*). Consistent with the reporter mice, *gp130flox/flox; SM22α-Cre* mice lacked gp130 expression in a subset of CD4$^+$ T cells (Fig. 3 *B* and *C*). By contrast, in *gp130flox/flox; CD4-Cre* mice (24), gp130 expression in CD4$^+$ T cells was almost completely absent, while IL-6Rα expression was retained (Fig. 3 *B–D*). In control *gp130flox/flox* mice, 60% of CD4$^+$ T cells expressed both gp130 and IL-6Rα, whereas these double-positive cells were almost absent in *gp130flox/flox; CD4-Cre* mice (Fig. 3 *E* and *F*). CD8$^+$ T cells showed a low abundance of IL-6Rα expression, even in control *gp130flox/flox* mice. The proportion of double-positive cells did not change in cells, other than CD3ε$^+$ T cells, depending on the presence of *CD4-Cre* (Fig. 3 *E* and *F*).

To characterize CD4$^+$ T cells as potential targets of *SM22α-Cre,* we sorted tdTomato-positive and tdTomato-negative CD4$^+$ T cells derived from the spleens of *SM22α-Cre* reporter mice and performed RNA-seq analysis (*SI Appendix*, Fig. S3*A*). We found only three genes as a significant difference between the two groups (tdTomato$^+$ up gene: 2 genes, tdTomato$^-$ up gene: 1 gene), indicating that there is little difference in gene expression between the tdTomato-positive and -negative CD4$^+$ T cells (*SI Appendix*, Fig. S3*B*). Consistently, the expression levels of the genes related to IL-6-signaling including *Il6st, Il6ra, Stat3, Jak1, Jak2,* and *Jak3* were almost comparable between the two groups (*SI Appendix*, Fig. S3*C*). We next analyzed the phosphorylation of STAT3 in the tdTomato-positive and -negative CD4$^+$ T cells derived from the lungs of *SM22α-Cre* reporter mice exposed to hypoxia (*SI Appendix*, Fig. S3*D*). Hypoxia exposure caused stronger tyrosine-phosphorylation of STAT3 in the tdTomato-positive CD4$^+$ T cells than in the tdTomato-negative CD4$^+$ T cells (*SI Appendix*, Fig. S3 *E* and *F*). Based on these results, we hypothesized that improvement of the HPH phenotype in *gp130flox/flox; SM22α-Cre* mice was due to unintended gp130 loss in CD4$^+$ T cells and that almost complete loss of gp130 expression in CD4$^+$

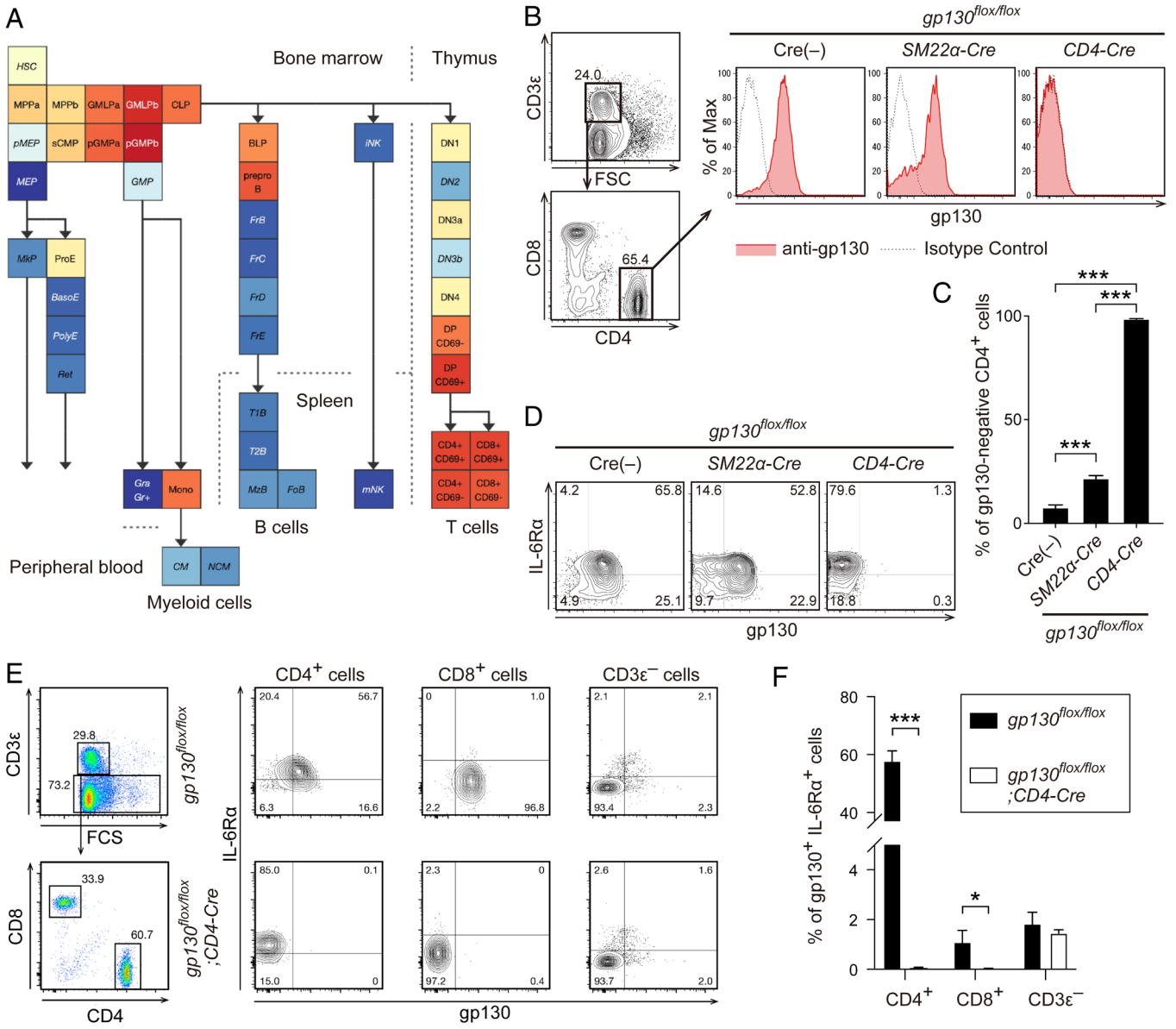

Fig. 3. Gp130 expression in CD4$^+$ T cells was partially abolished in *gp130flox/flox; SM22α-Cre* mice. (*A*) Mouse gp130 (IL6ST) expression pattern in hematopoietic lineage cells was retrieved using the mouse hematopoiesis model on Gene Expression Commons (23). (*B*) Representative flow cytometry analyses of gp130 expression patterns on CD3ε$^+$ CD4$^+$ T cells from the spleen of Cre(−) control, *gp130flox/flox; SM22α-Cre*, and *gp130flox/flox; CD4-Cre* mice are shown. Solid red lines and dashed black lines represent gp130 and background levels, respectively. (*C*) The percentages of gp130-negative cells in CD3ε$^+$ CD4$^+$ cells from the spleen of each mouse are shown. (*D*) Representative flow cytometry analyses of gp130 and IL-6Rα expression patterns on CD3ε$^+$ CD4$^+$ T cells from the spleen of *Cre(−)* control, *gp130flox/flox; SM22α-Cre*, and *gp130flox/flox; CD4-Cre* mice are shown. (*E*) Representative flow cytometry analyses of gp130 and IL-6Rα expression patterns on CD3ε$^+$ CD4$^+$, CD3ε$^+$ CD8$^+$, and CD3ε$^-$ cells from the spleen of Cre(−) control, *gp130flox/flox; SM22α-Cre*, and *gp130flox/flox; CD4-Cre* mice are shown. (*F*) The percentages of gp130$^+$ IL-6Rα$^+$ cells in CD3ε$^+$ CD4$^+$ cells from the spleen of each mouse are shown.

T cells in *gp130flox/flox; CD4-Cre* mice would result in further improvement of the HPH phenotype.

Gp130 Deletion in CD4$^+$ T Cells Ameliorated the PH Phenotype of HPH Mice. To determine the effect of gp130 deletion in CD4$^+$ T cells on the pathogenesis of PAH, we subjected *gp130flox/flox; CD4-Cre* mice to 4 wk of hypoxia. Hemodynamic studies revealed that RVSP was significantly reduced in *gp130flox/flox; CD4-Cre* mice compared with control *gp130flox/flox* mice (Fig. 4*A*). Right ventricular hypertrophy was comparable in both groups (Fig. 4*B*). Histological analysis showed a decrease in medial wall thickness in *gp130flox/flox; CD4-Cre* mice compared with control *gp130flox/flox* mice (Fig. 4*C*). These results indicated that gp130-dependent signaling in CD4$^+$ T cells plays a pivotal role in the pathogenesis of HPH.

We then examined how the loss of gp130 in CD4$^+$ T cells in the HPH model caused changes in downstream signaling. STAT3 is located downstream of gp130, and when IL-6 binds to the receptor, the JAK-STAT pathway is activated and STAT3 is phosphorylated. We previously reported that *Il6* mRNA expression in the lungs peaks on day 2 of hypoxic exposure (8). Therefore, we analyzed the phosphorylation of STAT3 in lung CD4$^+$ cells on day 3 of hypoxic exposure by flow cytometry. Hypoxic exposure caused STAT3 phosphorylation in CD4$^+$ T cells, which was completely suppressed by gp130 deletion in these cells (Fig. 4 *D* and *E*). Interestingly, phosphorylation of STAT3 was not observed in CD4$^+$ T cells in the spleen, suggesting that a gp130 ligand produced locally in the lungs was important (Fig. 4*F*). Because gp130 is a common subunit in IL-6 family cytokines, we examined the mRNA expression of IL-6 family cytokines in the lungs during

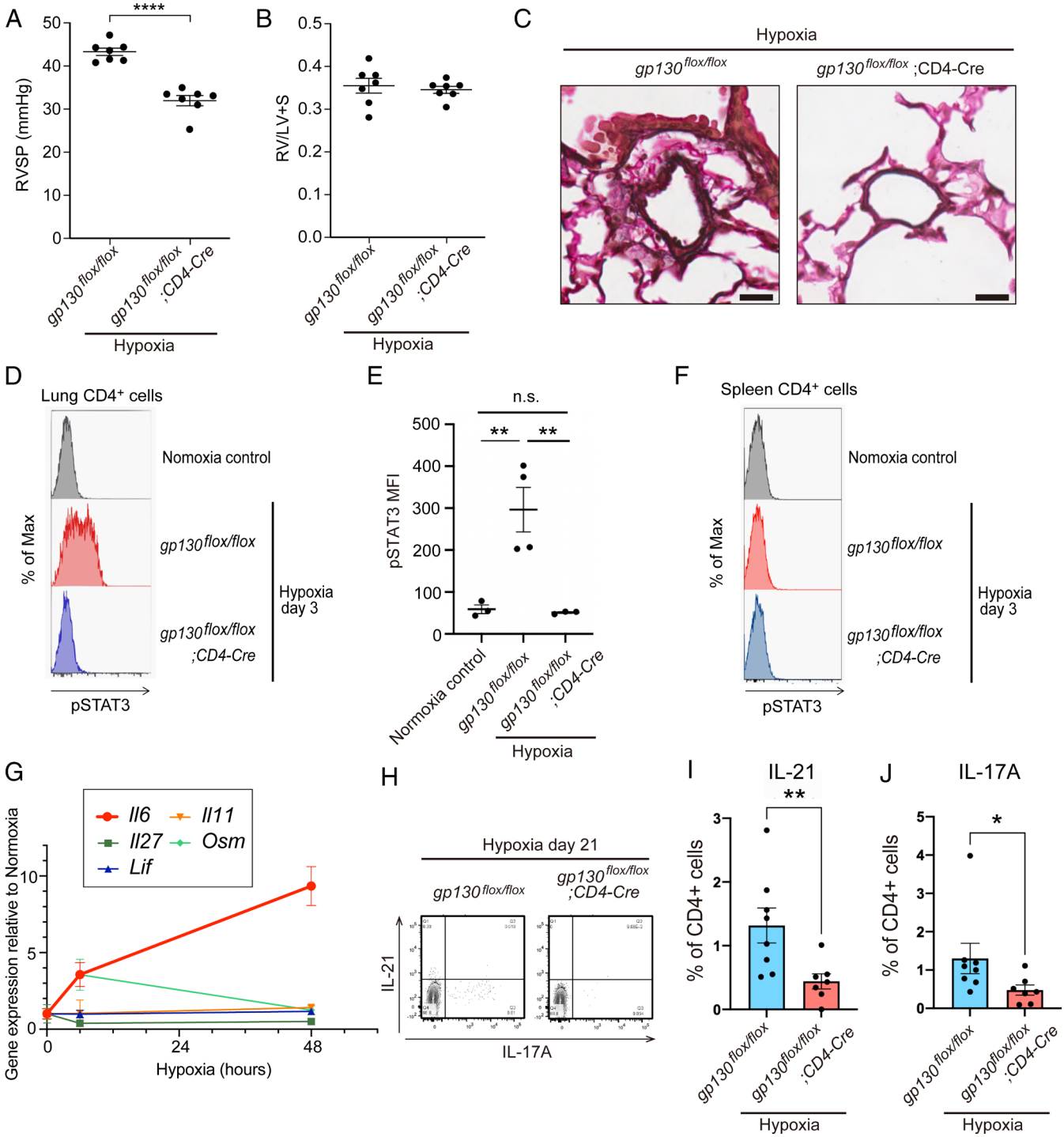

Fig. 4. Gp130 deletion in CD4$^+$ T cells ameliorated the PH phenotype of HPH mice. (*A*) Right ventricular systolic pressure of each group. (*B*) Right ventricle/left ventricle + septum (RV/LV+S) weight ratio (Fulton's index) of each group. (*C*) Representative images of pulmonary arteries with a diameter ~50 μm stained with Elastica van Gieson. (Scale bar: 20 μm.) (*D*) Phosphorylation of STAT3 (pSTAT3) in CD4$^+$ cells from the lungs of each mouse at hypoxia day 3 is shown. (*E*) Median fluorescence intensity (MFI) of pSTAT3 in CD4$^+$ cells from the lungs of each mouse at hypoxia day 3 is shown. (*F*) Phosphorylation of STAT3 (pSTAT3) in CD4$^+$ cells from the spleen of each mouse at hypoxia day 3 is shown. (*G*) mRNA expression levels of IL-6 family cytokines in the lungs of wild-type C57BL/6 mice after hypoxic exposure are shown. (*H*) Representative flow cytometry analysis of IL-17A and IL-21 expression in CD4$^+$ cells in the lungs at hypoxia day 21. (*I* and *J*) Percentages of IL-21$^+$ (*I*) and IL-17A$^+$ (*J*) cells among the CD4$^+$ cells at hypoxia day 21.

the acute phase of hypoxic exposure. Family cytokines other than IL-6 showed little increase in expression following hypoxic exposure (Fig. 4*G*). These results suggested that IL-6 is the cytokine responsible for gp130 signaling in CD4$^+$ T cells on hypoxic exposure. Th17 cells and IL-21-producing CD4$^+$ T cells were increased in the lungs during the acute phase of hypoxic exposure, but deletion of gp130 in CD4$^+$ T cells suppressed this increase (*SI Appendix*, Fig. S4 *A–C*). In the chronic phase of hypoxia, the increase in Th17 cells and IL-21-producing T cells was also suppressed by gp130 deletion in CD4$^+$ T cells (Fig. 4 *H–J*).

Genetic Deletion of *Il6* in Rats. The pathological features observed in severe cases of human PAH do not develop in mouse PH models. To test whether IL-6/gp130 signaling is also important in severe PH models, we generated *Il6* KO rats using the CRISPR-Cas9 system with a specific sgRNA-*rIl6* and *Cas9* mRNA, targeting

the second exon of the *Il6* gene. In one of the newborn rats, a deletion of 118 bp was found, which originated from an out-of-frame shift in the open reading frame that led to a premature stop codon and the generation of a completely different amino acid (aa) sequence (*SI Appendix*, Fig. S5*A*). To confirm IL-6 deficiency in the generated *Il6* KO rats, we examined the plasma IL-6 levels after LPS administration. Four hours after intraperitoneal LPS administration, there was a marked increase in plasma IL-6 levels in WT rats, but this increase was abolished in *Il6* KO rats (*SI Appendix*, Fig. S5*B*). We examined the tyrosine-phosphorylation of STAT3 in the lungs of each rat. Although tyrosine phosphorylation of STAT3 was strongly induced by LPS administration in the lungs of WT rats, it was attenuated in those of *Il6* KO rats (*SI Appendix*, Fig. S5*C*). Thus, the lack of IL-6 signaling in the created *Il6* KO rats was confirmed.

***Il6* KO Rats Are Resistant to HPH.** We evaluated the effect of chronic hypoxia on *Il6* KO rats (*SI Appendix*, Fig. S6*A*). WT rats exposed to hypoxia (10% O_2) for 3 wk exhibited significantly increased RVSP, Fulton's index, and medial wall thickness compared with rats exposed to normoxia. By contrast, the hypoxia-induced elevation of these parameters was inhibited significantly in *Il6* KO rats (*SI Appendix*, Fig. S6 *B* and *C*). Similarly, remodeling of the medial vascular walls following hypoxia exposure in WT rats was also inhibited significantly in the lungs of *Il6* KO rats (*SI Appendix*, Fig. S6 *D* and *E*). WT and *Il6* KO rats showed no difference in physiological parameters under normoxia. We examined IL-6 mRNA levels in the lungs of WT rats after exposure to hypoxia using quantitative RT-PCR (qRT-PCR). *Il6* mRNA levels peaked on day 7 after hypoxia exposure and did not return to basal levels even on day 21 (*SI Appendix*, Fig. S6*F*). We next examined tyrosine-phosphorylation of STAT3 in the lungs of WT and *Il6* KO rats. Although tyrosine-phosphorylation of STAT3 was strongly induced by hypoxic exposure in the lungs of WT rats after 7 d hypoxic exposure, it was reduced in *Il6* KO rats (*SI Appendix*, Fig. S6 *G* and *H*). These results suggested that *Il6* KO rats are resistant to HPH, similar to the findings in *Il6* KO mice (7).

***Il6* KO Rats Are Resistant to MCT-Induced PH.** We evaluated the effect of MCT administration on *Il6* KO rats (*SI Appendix*, Fig. S7*A*). Previous studies reported survival rates of around 30% in rats in the 35 d following MCT administration (25). In the present study, the survival rate in MCT-injected WT rats was 41% at 5 wk. Kaplan–Meier survival curves demonstrated that *Il6* deficiency significantly improved the survival rate in MCT rats compared with WT rats (*SI Appendix*, Fig. S7*B*). The PH-associated changes in RVSP were significantly ameliorated in MCT-administered *Il6* KO rats (*SI Appendix*, Fig. S7*C*). There was a trend for decreased right ventricular hypertrophy in *Il6* KO rats compared with WT rats but this did not reach significance (*SI Appendix*, Fig. S7*D*). The vascular thickening and lumen closure observed in WT rats receiving MCT were mitigated in *Il6* KO littermates (*SI Appendix*, Fig. S7 *E* and *F*). Similar to the lungs of WT rats during hypoxia, *Il6* mRNA expression was also examined in the lungs of WT rats after MCT administration using qRT-PCR. *Il6* mRNA levels continued to increase after MCT administration, rising approximately 20-fold after 4 wk (*SI Appendix*, Fig. S7*G*). We also examined the tyrosine-phosphorylation of STAT3 in MCT-treated rat lungs as well as in HPH model WT and *Il6* KO rat lungs. Although tyrosine-phosphorylation of STAT3 was strongly induced by 5 wk after MCT administration in WT rat lungs, it was decreased in *Il6* KO rat lungs (*SI Appendix*, Fig. S7 *H* and *I*). These results indicated that IL-6 plays an important role in PH pathogenesis in the MCT model as well as in the HPH model.

***Il6* KO Rats Are Resistant to SuHx-Induced Severe PH.** We next examined the effect of IL-6 deficiency on the PH phenotypes in the SuHx rat PH model (Fig. 5*A*). As previously reported, WT rats showed a marked increase in RVSP to about 100 mmHg and marked right heart hypertrophy at 8 wk in the SuHx model (Fig. 5 *B* and *C*). In pulmonary vascular remodeling, not only medial thickening but also an increase in the number of occluded vessels due to intimal proliferation and plexiform-like lesions were observed (Fig. 5 *D*–*F*). In *Il6* KO rats, there was a significant decrease in RVSP and right ventricular hypertrophy (Fig. 5 *B* and *C*). The medial wall thickness index of intra-acinar arterioles was considerably lower in *Il6* KO rats than in WT rats (Fig. 5 *D*–*F*). Furthermore, a significant reduction in the percentage of occluded vessels in the pulmonary vessels was observed in *Il6* KO rats. Similar to the lungs of WT rats during hypoxia, *Il6* mRNA expression was increased after exposure to hypoxia and did not return to basal levels even 8 wk after Su5416 administration (Fig. 5*G*). We examined tyrosine-phosphorylation of STAT3 in the lungs of SuHx WT and *Il6* KO rats as well as in the lungs of HPH and MCT rats and found that tyrosine phosphorylation of STAT3 was significantly induced in the lungs of WT rats at 8 wk in the SuHx model but was suppressed in *Il6* KO rats (Fig. 5 *H* and *I*). These findings indicated that IL-6 also plays an essential role in the pathogenesis of severe PH.

IL-6 Induces Accumulation of STAT3-Activated $CD4^+$ Cells around Pulmonary Vascular Lesions in SuHx Rats. Next, we performed immunohistological studies to determine the cells involved in IL-6 signaling in the SuHx rat model of severe PH. We coimmunostained SuHx rat lungs harvested at 8 wk with antibodies against phospho-STAT3 (pSTAT3) with αSMA, vWF, CD68, or CD4 (Fig. 5*J* and *SI Appendix*, Figs. S8 and S9*A*). The concomitant expression of pSTAT3 and αSMA, vWF, or CD68 was not detected in the pulmonary arteries of naïve rats (*SI Appendix*, Fig. S8). In SuHx rats, we found increased perivascular pSTAT3-positive cells in WT rats, but they did not merge with SMA, vWF, or CD68 (*SI Appendix*, Fig. S8). Further, $CD68^+$ and $CD4^+$ cells were found to be increased in the perivascular lungs of WT rats in the SuHx model, but only some $CD4^+$ cells merged with pSTAT3 (Fig. 5*J*). By contrast, in *Il6* KO rats, few $pSTAT3^+$ cells were observed around pulmonary vessels, and $CD68^+$ cells were also reduced. In particular, $CD4^+$ $pSTAT3^+$ cells were hardly detected around the arteries. We also confirmed that the pSTAT3 and IL-21 copositive cells around the pulmonary vessels that resulted in remodeling in the SuHx model seen in WT rats were rarely seen in *Il6* KO rats (*SI Appendix*, Fig. S8). We previously reported that activation of aryl hydrocarbon receptor (AHR), a nuclear receptor/transcription factor, induces upregulation of inflammatory signals and accumulation of $CD4^+$ IL-21^+ T Cells in vascular lesions in the advanced stage of SuHx rats (26). In this study, cells with nuclear copositivity of AHR and pSTAT3 were found to cluster around pulmonary vessels in SuHx rats (Fig. 5*J* and *SI Appendix*, Fig. S9*B*). These results suggested that IL-6 is involved in either proliferation or differentiation of helper T cells during the pathogenesis of PH and that the activation of AHR could trigger a positive feedback loop of Th17 cell differentiation by the IL-6/AHR signaling axis in PH.

IL-6 Induces Immunological Synapse Formation via a Th17 Differentiation Accompanied with Upregulation of Glycolysis in the Lungs of SuHx Rats. To elucidate the mechanisms underlying the IL-6-dependent development of severe PH phenotypes, including intimal and plexiform-like lesions that are observed in the advanced stage, RNA-seq was performed using the 1- and 8-wk lungs of SuHx rats (*SI Appendix*, Fig. S10*A*). We identified 343 and 390 genes that were down-regulated in *Il6* KO rats at

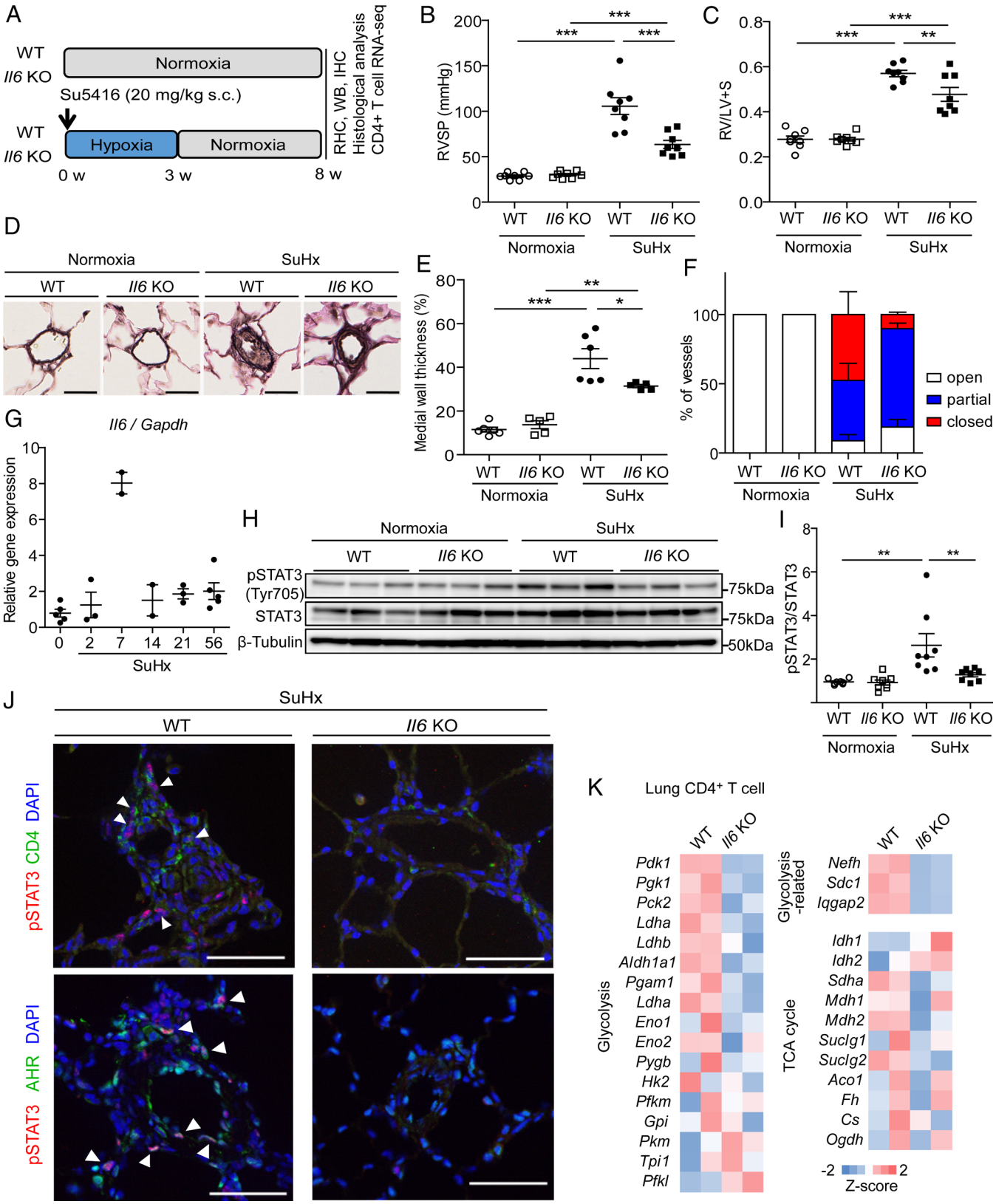

Fig. 5. *Il6* KO rats are resistant to PH in the SuHx rat model. (*A*) Experimental protocol for examining the effect of *Il6* deletion on SuHx rats. (*B* and *C*) Assessment of the effect of *Il6* deletion on the PH phenotype of SuHx rats in terms of RVSP (*B*) and Fulton's index (*C*) (n = 8 in each group). (*D*) Representative images of the vascular remodeling of distal acinar arterioles in lung sections subjected to EVG staining. (Scale bar: 20 μm.) (*E*) Medial wall thickness index of rats (normoxia WT: n = 6, normoxia *Il6* KO: n = 5, SuHx WT: n = 6, SuHx *Il6* KO: n = 5). (*F*) Pulmonary arterial occlusions were graded as open (no luminal occlusion; white), partial (<50% occlusion; blue), or closed (≥50% occlusion; red). Percentages of open, partial, and closed pulmonary arteries of outer diameter (OD) <100 μm in SuHx rats) (n = 4 in each group). (*G*) qRT-PCR analysis of *Il6* mRNA expression in the lungs of WT rats after SuHx treatment. (*H* and *I*) Western blot analysis of STAT3 phosphorylation (Tyr705) and total STAT3 in lung homogenates from WT and *Il6* KO rats 8 wk after normoxia or SuHx treatment (n = 8 in each group). (*J*) Representative immunofluorescence images of pulmonary arteries stained for pSTAT3 (red) and CD4 (green), and pSTAT3 (red) and Ahr (green) in the lung tissues of WT and *Il6* KO rats 8 wk after SU5416 administration. Arrowheads indicate copositive cells. (*K*) Z-score of respiration-related genes in $CD4^+$ cells. RHC: right heart catheterization, WB: western blotting, IHC: immunohistochemistry. Values are the means ± SEM. ***$P < 0.001$, **$P < 0.01$, and *$P < 0.05$.

1 and 8 wk, respectively, and 81 of these down-regulated genes were commonly detected at both time points (*SI Appendix*, Fig. S10 *B* and *C*). Pathway analysis using these 81 IL-6-dependent genes revealed upregulation of genes involved in immune cell dynamics (i.e., phagosome, antigen processing and presentation, and cell adhesion molecules) (*SI Appendix*, Fig. S10*D*). GO enrichment analysis using these 81 IL-6-dependent genes revealed upregulation of genes involved in immune cell accumulation (i.e., immune response, neutrophil chemotaxis, lymphocyte chemotaxis, antigen processing and presentation of peptide antigen via MHC class 1, and immunological synapse formation), indicating that the interaction of antigen-presenting cells such as B cells, macrophages, and dendritic cells with helper T cells occurred in an IL-6-dependent manner in SuHx rat lungs (*SI Appendix*, Fig. S10*E*). Because STAT3 activation was observed primarily in $CD4^+$ cells in the pulmonary perivasculature (Fig. 5*J*), we focused on $CD4^+$ cell-specific genes (*SI Appendix*, Fig. S10*F*). Twenty-two IL-6 dependently down-regulated genes were detected in $CD4^+$ cells (*SI Appendix*, Fig. S10*G*). Gene ontology (GO) enrichment analysis using the 22 genes down-regulated in $CD4^+$ cells revealed downregulation of several inflammation-associated biological processes (i.e., response to lipopolysaccharide, response to bacterium, and defense response to bacterium) (*SI Appendix*, Fig. S10*H*). Furthermore, pathway analysis using these 22 IL-6-dependent genes revealed downregulation of genes involved in inflammatory cell signaling (i.e., IL-17 signaling pathway and cell adhesion molecules) (*SI Appendix*, Fig. S10*I*). Because Th17 cells are characterized by distinctive homeostasis involving the upregulation of glycolysis (27–29), we focused on the metabolic genes associated with respiratory functions. Numerous glycolysis-related gene expressions exhibited downregulation in *Il6* KO rats, whereas the majority of TCA cycle gene expressions remain unaffected (Fig. 5*K*). These results suggest that immune cell activation, such as immunological synapse formation between T cells and APCs, is driven by IL-6 signaling-dependent glycolysis in T cells within the pulmonary lesions of severe PH models.

***Il6* Deficiency Suppresses Downregulation of BMPR2 Expression and Attenuates Apoptotic Signaling in the SuHx Model Lung.** We next examined the effects of IL-6 deficiency on bone morphogenetic protein receptor 2 (BMPR2) expression levels and apoptotic signaling, which have been shown to be associated with PH pathology. We found reduced levels of BMPR2 in the lung tissue protein lysate of SuHx WT rats at 8 wk (*SI Appendix*, Fig. S11*A*). The decrease in BMPR2 was suppressed in *Il6* KO rats (*SI Appendix*, Fig. S11*B*). In addition, the levels of cleaved caspase-3 and p53 were increased in the lung tissue of SuHx WT rats at week 8, and these increases were suppressed in *Il6* KO rats (*SI Appendix*, Fig. S11 *C* and *D*). Taken together, our data indicate that IL-6 deficiency suppresses both BMPR2 reduction and apoptotic responses in SuHx rat lungs.

***Il6* Deficiency and Standard Vasodilator Treatment Show an Additive Effect on the Pathogenesis of PH.** We examined whether IL-6 blockade has an additive effect on existing therapeutic agents, endothelin receptor antagonist (ERA), macitentan, and soluble guanylyl cyclase (sGC) stimulator, BAY41-2272. Rats were exposed to Su5416 and hypoxia (10%) for 3 wk before returning to room air for 2 wk to allow for the progression of pulmonary vascular remodeling. WT and *Il6* KO rats were then randomly divided into three groups to receive a pulverized chow containing macitentan (30 mg/kg/d) or BAY41-2272 (10 mg/kg/d), or a control diet, from week 5 for 3 wk (Fig. 6 *A* and *F*). The treatment of WT SuHx rats with macitentan or BAY41-2272 resulted in comparable attenuation of the PH phenotype. RVSP and right ventricular hypertrophy were also significantly reduced in *Il6* KO rats given a control diet. There were no significant effects on mean arterial pressure and heart rate indicating specific effects on pulmonary circulation. Interestingly, treatment of *Il6* KO rats with macitentan or BAY41-2272 resulted in a further reduction of RVSP and right ventricular hypertrophy compared with the WT rats treated with the respective drugs (Fig. 6 *B*, *C*, *G*, and *H*). Histological analysis of the lungs suggested that the hemodynamic changes caused by ERA or sGC stimulator treatment with IL-6 deficiency were associated with a reduction in medial wall thickness and the percentage of occluded vessels (Fig. 6 *D*, *E*, *I*, and *J*). These results suggest that IL-6 inhibition and existing anti-PAH drugs can be expected to have an additive inhibitory effect on the pathogenesis of PAH.

Discussion

In the present study, we used mouse and rat PH models to show that IL-6/gp130 signaling is important in the pathogenesis of PH. Phosphorylation of STAT3, a downstream molecule of IL-6/gp130 signaling, was observed in $CD4^+$ T cells in the lungs of both mouse and rat PH models. We also showed that $CD4^+$ T cells are an important target of IL-6 in the pathogenesis of PH in a tissue-specific gp130-deficient HPH mouse model. Deletion of gp130 in $CD4^+$ T cells suppressed phosphorylation of STAT3 and Th17 subsequently increased following hypoxic exposure, contributing to amelioration of the PH phenotype.

A recent clinical study examining the effects of tocilizumab, an anti-IL-6 receptor monoclonal antibody, in patients with group 1 PAH reported that treatment with tocilizumab was feasible but demonstrated no significant effect on hemodynamics (30). Because IL-6 is a multifaceted cytokine, it may have opposite effects on PAH depending on the cell type. Indeed, despite our study showing that blocking IL-6 signaling specifically in $CD4^+$ T cells improved the HPH phenotype in mice, another group reported that disrupting IL-6 signaling in SMCs using *SMMHC-CreERT2* mice worsened the phenotype (12). The balance of protective or promotive effects of IL-6 signaling on PH phenotypes by cell type may differ among species or PH models. Cell type-specific inhibition of IL-6 signaling, or inhibition of downstream molecules of IL-6 signaling in $CD4^+$ T cells, may be alternative strategies.

A previous study using *SM22α-Cre* mice to analyze the effects of tissue-specific IL-6α deficiency reported that smooth muscle is a target for IL-6 in the pathogenesis of PH (13). However, previous reports and our results show that some degree of non-specific *Cre* recombination also occurs in hematopoietic cells in *SM22α-Cre* mice (15), and the results should be interpreted with caution. Although a previous report showed that *SM22α-Cre* mice showed *Cre* recombination in only myeloid lineage cells, not in lymphoid lineage cells (15), our data showed that *Cre* recombination occurred to some extent even in the most undifferentiated hematopoietic stem cell stage, and as differentiation progressed, cells with *Cre* recombination accumulated. Our study showed that $CD4^+$ cells from the spleen did not show substantial difference in gene expression dependent on the *SM22α-Cre*-dependent recombination. On the other hand, hypoxia exposure to mice induced significant tyrosine-phosphorylation of STAT3 more strongly in the $CD4^+$ cells positive for *SM22α-Cre*-dependent recombination than in those negative for *SM22α-Cre*-dependent recombination. These data suggest that attenuation of the HPH phenotypes observed in the previous study and in our study using *SM22α-Cre* mice might be attributed to more preferential attenuation of IL-6-dependent signaling in the $CD4^+$ cells (13).

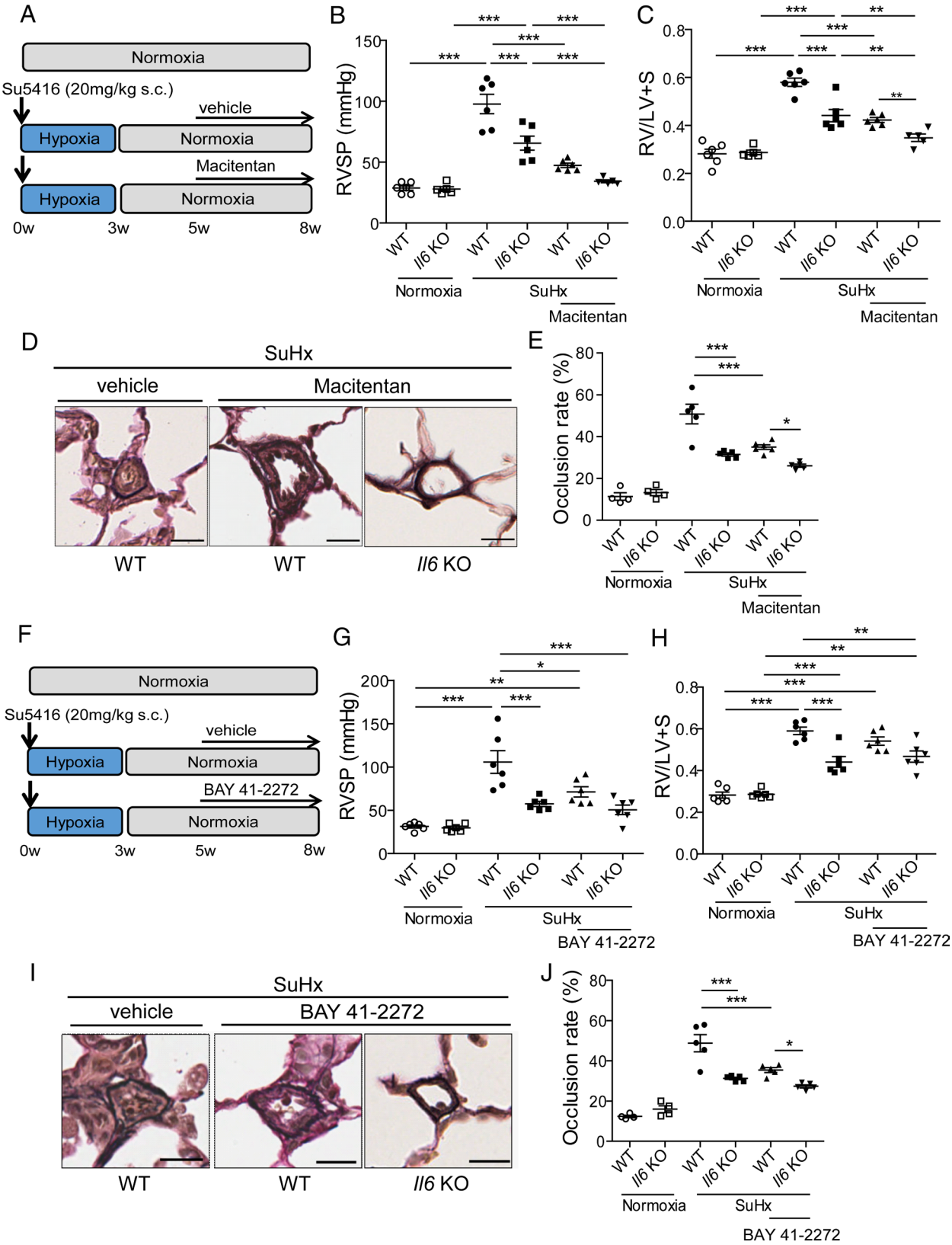

Fig. 6. *Il6* deficiency and standard of care vasodilator therapy combination in rats with SuHx-induced PH. (*A*) Experimental protocol for disease initiation and the macitentan treatment time course. A macitentan-containing diet (30 mg/kg/d) or a control diet was fed to rats every day. (*B* and *C*) Assessment of the effect of *Il6* deletion combined with macitentan treatment on the PH phenotype of SuHx rats in terms of RVSP (*B*) and Fulton's index (*C*) (normoxia WT: n = 6, normoxia *Il6* KO: n = 5, SuHx WT: n = 6, SuHx *Il6* KO: n = 6, SuHx+macitentan WT: n = 6, SuHx+macitentan *Il6* KO: n = 5). (*D*) Representative images of the vascular remodeling of distal acinar arterioles in lung sections subjected to EVG staining. (Scale bar: 20 μm.) (*E*) Vascular occlusion rate of rats (normoxia WT: n = 4, normoxia *Il6* KO: n = 4, SuHx WT: n = 5, SuHx *Il6* KO: n = 5, SuHx+macitentan WT: n = 5, SuHx+macitentan *Il6* KO: n = 5). (*F*) Experimental protocol for disease initiation and the macitentan treatment time course. A BAY41-2272-containing diet (10 mg/kg/d) or a control diet was fed to rats every day. (*G* and *H*) Assessment of the effect of *Il6* deletion combined with BAY41-2272 treatment on the PH phenotype of SuHx rats in terms of RVSP (*G*) and Fulton's index (*H*) (n = 6 in each group). (*I*) Representative images of the vascular remodeling of distal acinar arterioles in lung sections subjected to EVG staining. (Scale bar: 20 μm.) (*J*) Vascular occlusion rate of rats (normoxia WT: n = 4, normoxia *Il6* KO: n = 4, SuHx WT: n = 5, SuHx *Il6* KO: n = 5, SuHx+BAY41-2272 WT: n = 5, SuHx+BAY41-2272 *Il6* KO: n = 5). Values are the means ± SEM. ***$P < 0.001$, **$P < 0.01$, and *$P < 0.05$.

To compensate for the inability to induce severe lung lesions in mouse PH models, we generated *Il6* KO rats using the CRISPR/Cas9 system and examined the effects of IL-6 deficiency on conventional animal models of PH, such as the chronic hypoxia-induced PH model, the MCT-induced PH model, and the recently developed SuHx PH rat model, which exhibits plexiform-like lesions similar to those seen in patients with severe PAH. We found that in these three PH models, *Il6* KO rats showed a significant improvement in PH pathology. In addition, RNA-seq analysis revealed IL-6-dependent immunological synapse formation in SuHx model lungs. Furthermore, inflammatory cells such as macrophages and helper T cells that congregate around pulmonary blood vessels were rarely observed in *Il6* KO rats. In addition, the decreased expression levels of BMPR2 and increased apoptotic signaling associated with PH pathology observed in the lungs of WT rats were suppressed in the lungs of *Il6* KO rats. Furthermore, the additive effect of IL-6 deficiency with existing PAH therapies was also revealed. These results suggest that the IL-6 signaling pathway may be a promising therapeutic target in the treatment of mild to severe PH.

Inflammatory processes are thought to be prominent in various types of human PAH and experimental PH and are recognized as major pathogenic components of pulmonary vascular remodeling. Our group and others have shown that IL-6 plays an important role in PH pathogenesis in a murine HPH model. The response to hypoxia varies among animal species, and in particular, it has been reported that the mesangial thickening of pulmonary vessels in the rat HPH model is more severe than that in mice (31). In the present study, we found that IL-6 plays an important role in the pathogenesis of PH in HPH in rats as well as in mice. We have previously shown that *Il6* mRNA expression in the lungs of HPH mice peaks on day 2 after exposure to hypoxia and returns to basal levels on day 7. Further, we have shown that IL-6 mRNA expression in the lungs of the rat HPH model peaks on day 7 of hypoxic challenge and does not recover to baseline even after 21 d. These differences in IL-6 kinetics may contribute to the differences between mice and rats in the formation of pulmonary vascular remodeling in the HPH model.

Next, we examined the effects of IL-6 deficiency in another classic PH model, the MCT rat model. We observed a significant improvement in mortality and a significant decrease in RVSP in *Il6* KO rats after MCT administration. This and other previous studies have shown that *Il6* mRNA increases in a time-dependent manner in the lungs of MCT models (32). Furthermore, STAT3 phosphorylation in the lungs occurs in WT rats. Tamura et al. showed that administration of IL-6R/sIL6R antagonists significantly improved PH pathology in the MCT model (13). These results indicate that IL-6 is also important for the development of PH in the MCT model.

Furthermore, we investigated the effect of IL-6 deficiency in the SuHx model, which exhibits pulmonary vascular lesions similar to those of severe PAH in humans, and found that the PAH pathology in the SuHx model was markedly suppressed in *Il6* KO rats. In the SuHx model, the localization of phosphorylated STAT3 in the lungs was examined by immunohistological staining to clarify the target cells of IL-6. The results showed that there was little colocalization of phosphorylated STAT3 in remodeled pulmonary vascular smooth muscle, as previously reported (13), and that it merged into a subset of $CD4^+$ cells. IL-6, in cooperation with TGF-β, is reported to be critical for the differentiation of Th17 cells from naive $CD4^+$ T cells (33–35). We previously showed that Th17 cells ($CD4^+$ $IL\text{-}21^+$ $IL\text{-}17^+$ T cells) accumulated in the lung vascular lesions of HPH mice (8). In addition, we recently reported that activation of AHR plays an essential role in the pathogenesis of PH in the SuHx rat model (26). IL-6-dependent expression of AHR is crucial for the differentiation of Th17 cells, and AHR agonists promote Th17 cell differentiation induced by a combination of IL-6 and TGF-β (36, 37). In the present study, $IL\text{-}21^+$ cells around pulmonary vessels, which resulted in remodeling in the SuHx model in WT rats, were rarely seen in *Il6* KO rats. mRNA levels of genes involved in glycolysis, which is enhanced during differentiation of Th17 cells (27–29), were up-regulated in an IL-6-dependent manner in $CD4^+$ cells of the SuHx lungs. Taken together, these results suggest that activation of AHR triggers a positive feedback loop of Th17 cell differentiation via the IL-6/AHR signaling axis in PAH. It is necessary to mention the limitation of the present study. Although we showed STAT3 activation in the $CD4^+$ cells around the occlusive pulmonary arteries of the SuHx rats in immunohistochemistry and IL-6-dependent Th17 cell differentiation through RNA-seq analysis, we could not provide direct evidence for the necessity for $CD4^+$ cells in rat severe PAH models due to lack of *Cre-loxP* system in rats. Creation of the rat *Cre-loxP* system will make it possible to demonstrate the indispensability of $CD4^+$ cells downstream of IL-6-signaling in rat PAH models.

IL-6 has been shown to suppress BMPR2, one of the major disease-related genes in hereditary PAH, through overexpression of miR17/92 (38). Consistent with this finding, the decrease in BMPR2 expression in the lungs of the SuHx model was significantly suppressed in *Il6* KO rats. Although the underlying mechanisms remain unclear, dysfunctional BMPR2 signaling is known to be involved in sustained inflammation and impaired resolution. Endothelial cells from PAH patients with BMPR2 mutations exhibit enhanced proliferation, altered glucose metabolism, reduced monolayer integrity, and increased susceptibility to apoptosis (39, 40). Consistent with this finding, apoptotic signaling was enhanced in the lungs of WT rats of the SuHx model but was significantly suppressed in the lungs of *Il6* KO rats with normalized BMPR2 expression.

In conclusion, our findings indicate that gp130/IL-6 signaling in $CD4^+$ T cells plays an important role in the pathogenesis of PH and suggest that IL-6 blockade concurrent with existing treatments may be effective in patients with PAH.

Materials and Methods

In mice, hypoxia-induced pulmonary hypertension model was evaluated in *gp130flox/flox* (control) mice (19)and gp130 conditional KO mice using the tissue-specific Cre mouse such as *VE-Cad-CreERT2* mice (20), *SMMHC-CreERT2* mice (12, 21), *SM22α-Cre* mice (13, 16) and *CD4-Cre* mice (24), on a C57BL/6 background. In rats, hypoxia-induced, monocrotaline-induced, and SuHx-induced pulmonary hypertension models were examined using WT and *Il6* KO rats generated using the CRISPR-Cas9 system in an SD background. All experiments were carried out under the guidelines of the Animal Ethics Committee of the National Cerebral and Cardiovascular Center Research Institute and were also approved by the Institutional Review Board of the National Cerebral and Cardiovascular Center.

Data, Materials, and Software Availability. RNA-seq data have been deposited at GEO (https://www.ncbi.nlm.nih.gov/geo/) under accession number GSE255994 (41). All other data are included in the manuscript and/or *SI Appendix*.

ACKNOWLEDGMENTS. We thank Yuko Iwai and Nao Araki for secretarial assistance; Manami Nishimura, Saori Mizushima, and Mika Ejiri for technical assistance; and Manami Sone for technical assistance with histological analyses. We also thank Dr. Werner Müller (University of Manchester) for providing *gp130flox* mice. We

also thank Pharma Foods International Co., Ltd. (Kyoto, Japan) for the creation of the *Il6* KO rats. We thank Janssen Pharmaceutical K.K., Japan, and Bayer AG for providing macitentan and BAY41-2272, respectively. This work was supported in part by JSPS KAKENHI (Grant Numbers 19K17622 and 21K08070 to T. Ishibashi; 19K08506 and 22K08144 to T. Inagaki; 22H04379 to T.C.-K.; 23K07568 to M.O.; and 16H05298 to Y.N.); by JST, PRESTO Grant Number JPMJPR13M5, Japan, to Y.N.; by the Intramural Research Fund for Cardiovascular Diseases of the National Cerebral and Cardiovascular Center (29-6-5 and 30-6-4 to T. Ishibashi and 30-2-3 to T. Inagaki); by The Cell Science Research Foundation to T. Inagaki; by research grant in pulmonary hypertension from Nippon Shinyaku Ltd. to R.A.; and by the Takeda Science Foundation, SENSHIN Medical Research Foundation, Daiichi Sankyo Foundation of Life Science, Smoking Research Foundation, the Uehara Memorial Foundation, Janssen Pharmaceutical K.K. Contracted Research Grant, Chugai Pharmaceutical Co., Ltd. Contracted Research Grant, and Kishimoto Foundation to Y.N. Y.N. granted from Bayer Yakuhin, Ltd., outside the submitted work.

Author affiliations: [a]Department of Vascular Physiology, National Cerebral and Cardiovascular Center Research Institute, Suita, Osaka 564-8565, Japan; [b]Department of Pathology, National Cerebral and Cardiovascular Center, Suita, Osaka 564-8565, Japan; [c]Department of Cardiovascular Medicine, National Cerebral and Cardiovascular Center, Suita, Osaka 564-8565, Japan; [d]Omics Research Center, National Cerebral and Cardiovascular Center, Suita, Osaka 564-8565, Japan; [e]Department of Anatomy, Keio University School of Medicine, Tokyo 160-8582, Japan; [f]Department of Immune Regulation, Immunology Frontier Research Center, Osaka University, Suita, Osaka 565-0871, Japan; [g]Department of Cardiovascular Medicine, Osaka University Graduate School of Medicine, Suita, Osaka 565-0871, Japan; and [h]Department of Molecular Imaging in Cardiovascular Medicine, Osaka University Graduate School of Medicine, Suita, Osaka 565-0871, Japan

1. P. Dorfmuller, F. Perros, K. Balabanian, M. Humbert, Inflammation in pulmonary arterial hypertension. *Eur. Respir. J.* **22**, 358–363 (2003).
2. R. T. Schermuly, H. A. Ghofrani, M. R. Wilkins, F. Grimminger, Mechanisms of disease: Pulmonary arterial hypertension. *Nat. Rev. Cardiol.* **8**, 443–455 (2011).
3. E. H. Choy *et al.*, Translating IL-6 biology into effective treatments. *Nat. Rev. Rheumatol.* **16**, 335–345 (2020).
4. T. Kishimoto, Interleukin-6: Discovery of a pleiotropic cytokine. *Arthritis Res. Ther.* **8**, S2 (2006).
5. E. Soon *et al.*, Elevated levels of inflammatory cytokines predict survival in idiopathic and familial pulmonary arterial hypertension. *Circulation* **122**, 920–927 (2010).
6. M. K. Steiner *et al.*, Interleukin-6 overexpression induces pulmonary hypertension. *Circ. Res.* **104**, 236–244, 228p following 244 (2009).
7. L. Savale *et al.*, Impact of interleukin-6 on hypoxia-induced pulmonary hypertension and lung inflammation in mice. *Respir. Res.* **10**, 6 (2009).
8. T. Hashimoto-Kataoka *et al.*, Interleukin-6/interleukin-21 signaling axis is critical in the pathogenesis of pulmonary arterial hypertension. *Proc. Natl. Acad. Sci. U.S.A.* **112**, E2677–E2686 (2015).
9. H. Mori *et al.*, Pristane/hypoxia (PriHx) mouse as a novel model of pulmonary hypertension reflecting inflammation and fibrosis. *Circ. J.* **84**, 1163–1172 (2020).
10. K. Matsushita *et al.*, Zc3h12a is an RNase essential for controlling immune responses by regulating mRNA decay. *Nature* **458**, 1185–1190 (2009).
11. A. Yaku *et al.*, Regnase-1 prevents pulmonary arterial hypertension through mRNA degradation of interleukin-6 and platelet-derived growth factor in alveolar macrophages. *Circulation* **146**, 1006–1022 (2022).
12. C. Mickael *et al.*, IL-6Ra in smooth muscle cells protects against schistosoma- and hypoxia-induced pulmonary hypertension. *Am. J. Respir. Cell Mol. Biol.* **61**, 123–126 (2019).
13. Y. Tamura *et al.*, Ectopic upregulation of membrane-bound IL6R drives vascular remodeling in pulmonary arterial hypertension. *J. Clin. Invest.* **128**, 1956–1970 (2018).
14. P. Boucher, M. Gotthardt, W. P. Li, R. G. Anderson, J. Herz, LRP: Role in vascular wall integrity and protection from atherosclerosis. *Science* **300**, 329–332 (2003).
15. Z. Shen *et al.*, Smooth muscle protein 22 alpha-Cre is expressed in myeloid cells in mice. *Biochem. Biophys. Res. Commun.* **422**, 639–642 (2012).
16. R. Holtwick *et al.*, Smooth muscle-selective deletion of guanylyl cyclase-A prevents the acute but not chronic effects of ANP on blood pressure. *Proc. Natl. Acad. Sci. U.S.A.* **99**, 7142–7147 (2002).
17. J. Huang *et al.*, Angiotensin-converting enzyme-induced activation of local angiotensin signaling is required for ascending aortic aneurysms in fibulin-4-deficient mice. *Sci. Transl. Med.* **5**, 183ra158, 111–181 (2013).
18. G. Hansmann *et al.*, An antiproliferative BMP-2/PPARgamma/apoE axis in human and murine SMCs and its role in pulmonary hypertension. *J. Clin. Invest.* **118**, 1846–1857 (2008).
19. U. A. Betz *et al.*, Postnatally induced inactivation of gp130 in mice results in neurological, cardiac, hematopoietic, immunological, hepatic, and pulmonary defects. *J. Exp. Med.* **188**, 1955–1965 (1998).
20. K. Okabe *et al.*, Neurons limit angiogenesis by titrating VEGF in retina. *Cell* **159**, 584–596 (2014).
21. A. Wirth *et al.*, G12–G13-LARG-mediated signaling in vascular smooth muscle is required for salt-induced hypertension. *Nat. Med.* **14**, 64–68 (2008).
22. L. Madisen *et al.*, A robust and high-throughput Cre reporting and characterization system for the whole mouse brain. *Nat. Neurosci.* **13**, 133–140 (2010).
23. J. Seita *et al.*, Gene expression commons: An open platform for absolute gene expression profiling. *PLoS One* **7**, e40321 (2012).
24. P. P. Lee *et al.*, A critical role for Dnmt1 and DNA methylation in T cell development, function, and survival. *Immunity* **15**, 763–774 (2001).
25. T. Itoh *et al.*, C-type natriuretic peptide ameliorates monocrotaline-induced pulmonary hypertension in rats. *Am. J. Respir. Crit. Care Med.* **170**, 1204–1211 (2004).
26. T. Masaki *et al.*, Aryl hydrocarbon receptor is essential for the pathogenesis of pulmonary arterial hypertension. *Proc. Natl. Acad. Sci. U.S.A.* **118**, e2023899118 (2021).
27. V. A. Gerriets *et al.*, Metabolic programming and PDHK1 control CD4+ T cell subsets and inflammation. *J. Clin. Invest.* **125**, 194–207 (2015).
28. L. Z. Shi *et al.*, HIF1alpha-dependent glycolytic pathway orchestrates a metabolic checkpoint for the differentiation of TH17 and Treg cells. *J. Exp. Med.* **208**, 1367–1376 (2011).
29. Z. Zhao *et al.*, The PRAK-NRF2 axis promotes the differentiation of Th17 cells by mediating the redox homeostasis and glycolysis. *Proc. Natl. Acad. Sci. U.S.A.* **120**, e2212613120 (2023).
30. M. Toshner *et al.*, Mendelian randomisation and experimental medicine approaches to interleukin-6 as a drug target in pulmonary arterial hypertension. *Eur. Respir. J.* **59**, 2002463 (2022).
31. Y. Hoshikawa *et al.*, Hypoxia induces different genes in the lungs of rats compared with mice. *Physiol. Genomics* **12**, 209–219 (2003).
32. C. Tang *et al.*, Characteristics of inflammation process in monocrotaline-induced pulmonary arterial hypertension in rats. *Biomed. Pharmacother.* **133**, 111081 (2021).
33. E. Bettelli *et al.*, Reciprocal developmental pathways for the generation of pathogenic effector TH17 and regulatory T cells. *Nature* **441**, 235–238 (2006).
34. P. R. Mangan *et al.*, Transforming growth factor-beta induces development of the T(H)17 lineage. *Nature* **441**, 231–234 (2006).
35. M. Veldhoen, R. J. Hocking, C. J. Atkins, R. M. Locksley, B. Stockinger, TGFbeta in the context of an inflammatory cytokine milieu supports de novo differentiation of IL-17-producing T cells. *Immunity* **24**, 179–189 (2006).
36. A. Kimura, T. Naka, K. Nohara, Y. Fujii-Kuriyama, T. Kishimoto, Aryl hydrocarbon receptor regulates Stat1 activation and participates in the development of Th17 cells. *Proc. Natl. Acad. Sci. U.S.A.* **105**, 9721–9726 (2008).
37. T. Nakahama *et al.*, Aryl hydrocarbon receptor-mediated induction of the microRNA-132/212 cluster promotes interleukin-17-producing T-helper cell differentiation. *Proc. Natl. Acad. Sci. U.S.A.* **110**, 11964–11969 (2013).
38. M. Brock *et al.*, Interleukin-6 modulates the expression of the bone morphogenic protein receptor type II through a novel STAT3-microRNA cluster 17/92 pathway. *Circ. Res.* **104**, 1184–1191 (2009).
39. I. Diebold *et al.*, BMPR2 preserves mitochondrial function and DNA during reoxygenation to promote endothelial cell survival and reverse pulmonary hypertension. *Cell Metab.* **21**, 596–608 (2015).
40. L. Long *et al.*, Selective enhancement of endothelial BMPR-II with BMP9 reverses pulmonary arterial hypertension. *Nat. Med.* **21**, 777–785 (2015).
41. T. Ishibashi *et al.*, Data from "IL-6/gp130 signaling in CD4+ T cells drives the pathogenesis of pulmonary hypertension". Gene Expression Omnibus. https://www.ncbi.nlm.nih.gov/geo/query/acc.cgi?acc=GSE255994. Deposited 16 February 2024.